

High-Stress Si_3N_4 Reflective Membranes Monolithically Integrated with Cavity Bragg Mirrors

Megha Khokhar,^{1,2} Lucas Norder,¹ Paolo M. Sberna,^{3,*} and Richard A. Norte^{1,†}

¹*Department of Precision and Microsystems Engineering,
Delft University of Technology, Delft 2628 CD, The Netherlands*

²*Kawli Institute of Nanoscience, Department of Quantum Nanoscience,
Delft University of Technology, Delft 2628 CD, The Netherlands*

³*Euse Kooi Laboratory, Faculty of Electrical Engineering, Mathematics and Computer Science,
Delft University of Technology, Delft 2628 CD, The Netherlands*

(Dated: March 4, 2026)

High-stress silicon nitride (Si_3N_4) membranes represent the state-of-the-art for cavity optomechanics, combining ultralow dissipation, optical transparency, and full compatibility with wafer-scale nanofabrication. Yet their integration into high-finesse optical cavities has remained difficult, typically requiring bonding or alignment-sensitive assembly that limits scalability and long-term stability. Here, we introduce a monolithic, wafer-level integration strategy that directly suspends high-stress Si_3N_4 photonic-crystal membranes above thermally compatible SiN/SiO_2 distributed Bragg reflectors (DBRs) capable of withstanding the high temperatures required for stoichiometric Si_3N_4 growth. A defect-free amorphous-silicon sacrificial layer and stiction-free plasma undercut yield vertically coupled cavities with sub-micron spacing—forming self-aligned resonators within seconds of release. Owing to the intrinsic tensile stress, the suspended membranes exhibit atomic-scale sagging, ensuring near-ideal cavity parallelism and long-term stability. Optical reflectivity measurements reveal cavity finesse exceeding 8×10^2 with nanoscale gaps between mirrors. Mechanical ringdown measurements show $Q_{\text{mech}} > 10^9$, indicating that DBR integration preserves the low-dissipation character of high-stress Si_3N_4 . This demonstrates that the integration process preserves the material’s exceptional dissipation dilution, supporting straightforward extension to high-Q nanomechanical architectures reported in the literature. The resulting Si_3N_4 -DBR platform unites optical and mechanical coherence with high fabrication yield and design flexibility, enabling scalable optomechanical devices for precision sensing and quantum photonics.

I. INTRODUCTION

Cavity optomechanics, which leverages the interaction between light and mechanical motion in resonant systems, has emerged as a pivotal platform for both fundamental studies and precision sensing technologies [1, 2]. At its simplest, it consists of an optical cavity with one of its mirrors being movable. The mirror’s motion modulates the cavity field enabling exquisite readout of displacement and forces. Confining light within small volumes with high-finesse cavities further amplifies these effects, enabling ground-state cooling [3], quantum squeezing [4], and ultra-sensitive force [5] and some of the most sensitive displacement detection achieved in science [6]. Achieving such performance requires extreme optical and mechanical coherence: the cavity must maintain high finesse, and the mechanical element must exhibit ultralow mechanical dissipation and strong optomechanical coupling. To approach these limits, the movable mirror should combine high optical quality (high reflectivity and low curvature) with low mechanical loss, which in practice favors lightweight, high-stress membranes that can be engineered for minimal coupling to their supports.

Among available materials for such reflectors, high-

stress silicon nitride (Si_3N_4) membranes have emerged as a state of the art for room-temperature optomechanics [7]. Their combination of large built-in tensile stress [8], ultralow optical absorption at telecom wavelengths (parts per billion) [9], and wafer-scale CMOS manufacturing has enabled exceptional optomechanical performance (Q_{mech}) [10–17]. As a result, Si_3N_4 membranes enable attonewton-level force sensing, chip-scale inertial navigation [18], mechanical frequency combs [19], and quantum state preparation at room temperature [20]. Their versatility has enabled a wide range of nanomechanical geometries, including: strings [14, 15, 21–26], drumheads [10, 16, 27–29], phononic-crystal (PtC) resonators [11, 13, 17, 30, 31], and trampoline membranes [5, 12, 32, 33]. All examples exhibit record-low damping and strong isolation from room temperature thermomechanical noise.

A key ingredient behind this performance is the high-temperature Low Pressure Chemical Vapor Deposition (LPCVD) required to form stoichiometric Si_3N_4 with gigapascal tensile stress and parts-per-billion optical absorption [9]. These elevated temperatures achieve stoichiometry that suppresses absorption and yields a mechanical loss tangent among the lowest of any nanomechanical material in the kHz–MHz bending regime. While Si_3N_4 resonators already exhibit the highest Q_{mech} at room temperature, their quality factor increases even further at cryogenic temperatures [34–38], reinforcing

* p.m.sberna@tudelft.nl

† r.a.Norte@tudelft.nl

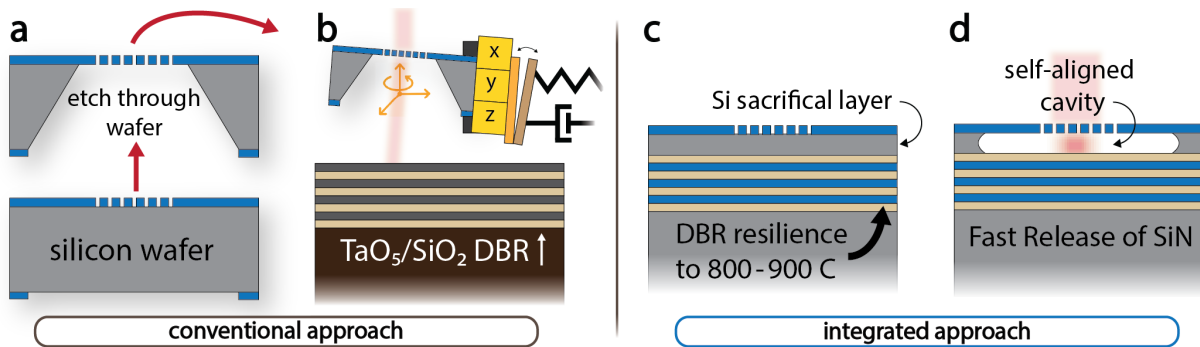


FIG. 1. Conventional fabrication of Si_3N_4 Membranes vs. integrated approach. (a) conventional fabrication of Si_3N_4 membranes for optical access requires deep etches through the chip which are complex, delicate and leave residues that must be subsequently cleaned off. (b) Complex alignment infrastructure to align with conventional DBR to form cavity. (c) integrated approach deposits high stress Si_3N_4 at high temperatures over Si sacrificial layer and DBR made from SiO_2 and Si_3N_4 . A few second undercut of Si layer suspended high stress Si_3N_4 photonic crystal membranes above DBR to form self-aligned, monolithic optomechanical cavity with a high Q_{mech} .

their role as a uniquely powerful platform for both quantum and precision sensing at all temperatures.

Such extreme mechanical sensitivity, however, demands an equally stable optical interface for readout. Achieving sub-nanometer alignment between reflective Si_3N_4 membranes and conventional mirrors requires exceptional mechanical precision and thermal stability, typically enforced by extensive alignment infrastructure [39–46]. As shown in FIG. 1a-b, Existing implementations often rely on fabrication schemes that etch completely through the Si_3N_4 chip to open an optical access window [47], followed by manual alignment of the membrane with an external cavity structure. These conventional approaches are delicate, time-consuming, and difficult to scale or package.

Recent efforts to integrate high-performance nanomechanical mirrors above distributed Bragg reflectors (DBRs) have explored sacrificial-layer deposition strategies, as demonstrated in III–V systems [48]. However, III–V platforms remain limited by small wafer formats, CMOS incompatibility, and mechanical properties that degrade over time. Extending similar integration schemes to Si_3N_4 has been fundamentally constrained by material incompatibility: the high temperatures ($\approx 800\text{--}900\text{ }^\circ\text{C}$) required for stoichiometric, high-stress Si_3N_4 growth exceed the thermal budget of conventional $\text{Ta}_2\text{O}_5/\text{SiO}_2$ DBRs, leading to film degradation and delamination. Attempts to directly bond Si_3N_4 membranes on mirrors have not maintained a high Q_{mech} [44, 49] and still required tedious alignment. These limitations have prevented the realization of a scalable, monolithic optomechanical cavity platform that maintains the exceptional optical and mechanical performance of Si_3N_4 membranes. Ultra-short cavity lengths have been long-sought for their ability to enhance optomechanical coupling in ways that depart from longer free-space cavities [46, 48]

In this work, we overcome these long-standing challenges by introducing a monolithic cavity platform

that directly integrates a suspended high-stress Si_3N_4 membrane above a thermally robust, low-loss LPCVD $\text{SiO}_2/\text{Si}_3\text{N}_4$ DBR. Using a defect-free amorphous-silicon sacrificial layer and a stiction-free dry plasma undercut, we achieve sub-micron cavity gaps between membrane reflector and DBR. These are self-aligned with nanoscale precision and are among the shortest free-space optomechanical cavities to date utilizing reflective Si_3N_4 membranes [46, 48, 49]. The suspended membranes with about 1 gigapascal of tensile stress exhibit picometer-scale sag on the order of an atomic radius, naturally producing parallel optical interfaces and high fabrication yield. This establishes a scalable route to compact, high-coherence Si_3N_4 cavity optomechanics without the alignment and assembly bottlenecks of conventional membrane-in-the-middle systems.

II. DESIGN AND OPTICAL OPTIMIZATION OF AN INTEGRATED OPTOMECHANICAL CAVITY

Optical cavity readout is achieved by vertically coupling a mechanically compliant Si_3N_4 PtC membrane to a high-reflectivity DBR, forming a compact Fabry–Pérot cavity (FIG. 2a). In this geometry, the suspended PtC serves as the partially transmitting top mirror and the DBR as the highly reflective bottom mirror, while the sub-micron air gap between them defines the optical cavity. Small membrane displacements modulate the cavity resonance frequency, enabling sensitive interferometric readout. The corresponding optomechanical coupling strength, $G = \partial\omega_c/\partial x$, increases as the optical mode volume is reduced, so tighter vertical confinement and smaller cavity gaps enhance displacement-to-frequency transduction.

First, the DBR is designed. The DBR is deposited across the full wafer and provides a broadband reflection band. We use alternating SiO_2 ($n_1 = 1.44$) and

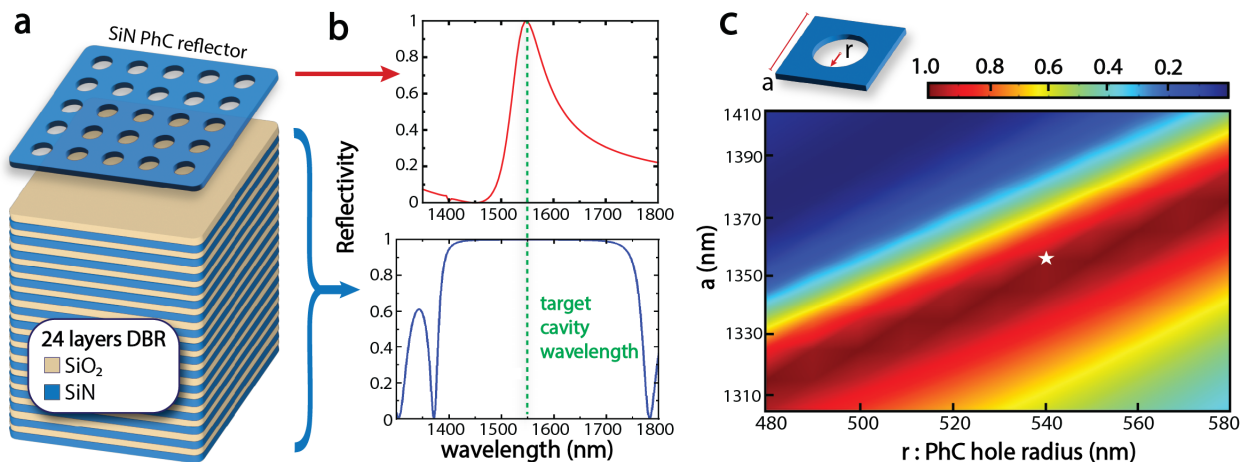


FIG. 2. Design and optical optimization of the integrated Si_3N_4 -DBR cavity. (a) Schematic of the cavity structure showing a high-stress Si_3N_4 PtC membrane suspended above a 24-layer $\text{Si}_3\text{N}_4/\text{SiO}_2$ distributed Bragg reflector (DBR). (b) Simulated reflectivity spectra of the PtC membrane (red) and the DBR (blue), showing their overlap at the target cavity wavelength of 1550 nm (green dashed line). (c) Simulated reflectivity contour map of the PtC as a function of lattice constant a and hole radius r , indicating the design point (white star) used for fabrication.

Si_3N_4 ($n_2 = 2.0$) quarter-wave layers centered at 1550 nm. Thicknesses of 269 nm (SiO_2) and 194 nm (Si_3N_4) yield constructive optical interference and a simulated peak reflectivity of $\approx 99.91\%$ for a 24-layer stack with total thickness ≈ 5.8 μm . The topmost layer is SiO_2 , which improves selectivity during the SF_6 release step, minimizes surface roughness, and ensures that the DBR remains optically pristine throughout processing. A representative DBR spectrum is shown in FIG. 2b.

The suspended membrane acts as a lithographically tunable photonic mirror: adjusting its PtC geometry allows fine control over its reflectivity and over the wavelength at which it overlaps the DBR stopband. We use a 200 nm-thick high-stress Si_3N_4 film, which balances reflectivity with mechanical dissipation (thinner membranes improve Q_{mech} but reduce achievable optical reflectivity).

Finite-element simulations (COMSOL) were used to obtain the reflectivity of the PtC by sweeping hole radius r and lattice constant a near the 1550 nm design point. The resulting reflectivity map (Fig. 2c) displays a narrow ridge of high reflectance corresponding to constructive out-of-plane interference. The geometry marked by the white star maximizes reflectivity while remaining robust against lithographic tolerances.

Because the PtC mirror relies on in-plane periodicity, it is naturally polarization dependent and its reflectivity varies with the incident beam's divergence. Larger, less focused beams sample more periods with a narrower in-plane k -distribution, improving effective reflectance. In contrast, the DBR has only vertical periodicity and is polarization insensitive, providing uniform broadband reflectivity.

To model the combined cavity, rigorous coupled-wave analysis (RCWA) is used. In this simulation, realis-

tic fabrication deviations from nominal values are included. Good agreement with simulations is obtained using the following representative parameters $a = 1.36$ μm , $r = 0.557$ μm , $t_{\text{SiN}} = 193$ nm, $t_{\text{SiO}} = 271$ nm, $n_{\text{SiN}} = 2.09$, $n_{\text{SiO}} = 1.42$, cavity spacing $t_{\text{cav}} \approx 0.95$ μm , and membrane thickness $t_{\text{PtC}} = 191$ nm. Small deviations arise naturally in LPCVD films but do not significantly impact finesse due to the broad DBR stopband and the gentle slope of the PtC reflectivity ridge.

Overall, the DBR provides a thermally robust, broadband mirror, while the lithographically tunable PtC allows precise spectral matching to the cavity wavelength. Together they form a monolithic, self-aligned cavity with strong vertical confinement suitable for high-sensitivity optomechanical readout. Vertical optomechanical coupling is particularly well matched to Si_3N_4 , since its highest- Q resonators rely on out-of-plane flexural modes set by ultrathin film thicknesses (≈ 200 nm), easily realized by deposition but very difficult to achieve through lateral nanolithography.

III. SCALABLE NANOFABRICATION USING DRY PROCESSING TECHNIQUES

To realize a robust, wafer-scale platform for monolithic optomechanical cavities, we developed a fabrication flow composed entirely of dry-processing steps (FIG. 3a), with both top- and cross-sectional views shown for each stage. Eliminating liquids in the fabrication process avoids stiction and capillary forces, ensuring that the pristine optical and mechanical properties of high-stress Si_3N_4 are fully preserved.

The process begins with LPCVD deposition of the multilayer $\text{Si}_3\text{N}_4/\text{SiO}_2$ DBR on a silicon wafer. Be-

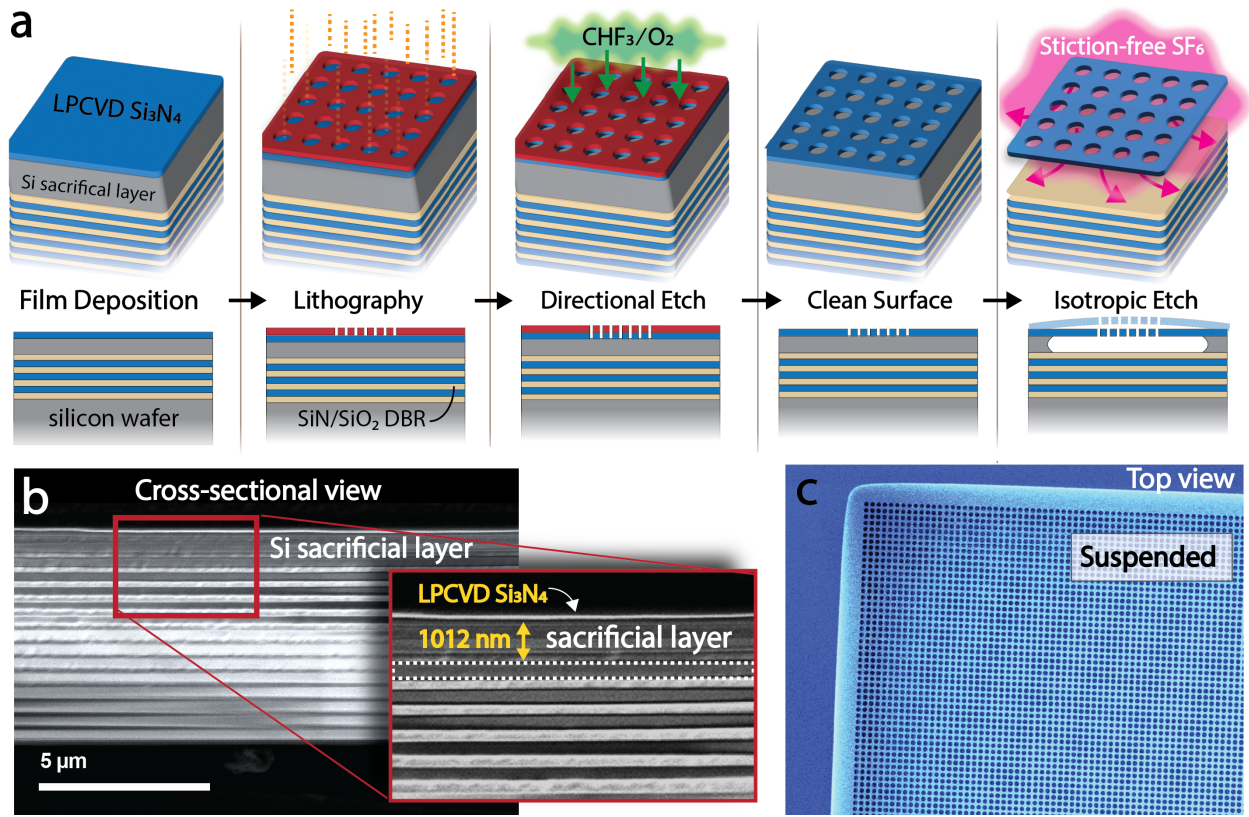


FIG. 3. **High-yield fabrication of monolithic Si_3N_4 -DBR optomechanical cavities.** (a) Schematic fabrication flow with top and side views for each step: LPCVD growth of the Si_3N_4 / SiO_2 DBR and amorphous-Si sacrificial layer; lithographic patterning of the Si_3N_4 membrane; directional CHF_3/O_2 etching; surface cleaning; and stiction-free isotropic SF_6 undercut to suspend the membrane. (b) Cross-sectional SEM showing the DBR stack, amorphous-Si sacrificial layer, and top Si_3N_4 membrane prior to release (inset: measured sacrificial-layer thickness ~ 1012 nm). The white dashed lines highlight the top SiO_2 layer of the DBR. (c) Top-view optical micrograph of the fully suspended membrane, demonstrating wafer-scale uniformity and clean release.

cause every layer is deposited at high temperature, the DBR maintains its structural stability and sharp interfaces throughout subsequent processing. 1012 nm of an amorphous-Si sacrificial layer is then deposited by Inductively Coupled Plasma - Chemical Vapor Deposition (ICP-CVD), with parameters tuned to suppress hydrogen incorporation and prevent blistering or bubble formation during the later high-temperature LPCVD step. Finally, a 200 nm stoichiometric Si_3N_4 layer is deposited to form the high-stress membrane and later patterned with nanoholes to increase its reflectivity. The full deposition recipes are detailed in Methods.

The membrane pattern is defined using high-resolution electron-beam lithography. After exposure and development, the square-lattice PtC holes are transferred into the Si_3N_4 layer using a CHF_3/O_2 Inductively Coupled Plasma Reactive Ion Etching (ICP-RIE) that provides anisotropic profiles and smooth sidewalls. Residual resist is removed with N,N -dimethylformamide, followed by a piranha clean to eliminate organics and leave a chemically pristine membrane surface prior to suspension.

Suspension is achieved through a short isotropic

SF_6 plasma undercut, which selectively removes the amorphous-Si layer while leaving both the membrane and DBR relatively unetched (FIG. 3a). Because the release is fully dry, the process is inherently stiction-free, enabling the fabrication of high-aspect-ratio suspended nanostructures with minimal collapse or fracturing [14, 17, 50]. The SF_6 undercut produces exceptionally clean cavity interfaces, uniform air gaps, and high repeatability across full wafers [51]. Importantly, this dry-release method has repeatedly been shown to produce nanomechanical devices with some of the lowest mechanical and optical losses to date, and with high-fidelity agreement between simulated and measured dissipation—performance that is difficult to achieve with liquid-based etches such as KOH, which can require hours of through-wafer etching to obtain optical access. In contrast, our cavities are formed in tens of seconds, immediately yielding a fully aligned Si_3N_4 membrane-DBR cavity; this represents a fundamental shift in how state-of-the-art membrane materials are integrated with readily available optical readout systems.

Cross-sectional SEM images (FIG. 3b) show the mul-

tilayer DBR, the sacrificial layer, and the sharpness of the interfaces produced by the LPCVD stack. Top-view images (FIG. 3c) show fully suspended membranes with uniform PtC patterns. The residual tensile stress of ≈ 1 GPa keeps the films taut, flat, and robust during handling and optical probing, with nanoscale sag across millimeter-scale spans [52], producing cavity parallelism between the membrane and DBR that would be infeasible to recreate with conventional alignment schemes as shown in FIG.1b.

Together, these dry-processing steps provide a high-yield, wafer-scale route to monolithic membrane-DBR cavities with robust structural integrity. We now show that the platform delivers more than mechanically surviving membranes: it also preserves strong optical cavity performance and low mechanical dissipation.

IV. CHARACTERIZATION OF OPTICAL CAVITY RESONANCES

To evaluate the optical performance of the integrated Si_3N_4 membrane-DBR cavity, we performed micro-reflectivity measurements using the setup shown in FIG. 4a. A tunable diode laser (1530–1620 nm) is routed through a collimator, polarization controller, and polarizer, then focused onto the membrane using a high-NA objective. Reflected light returns through the same optical path and is routed to a photodiode via a circulator. A white-light illumination path and camera are integrated into the beam path, enabling real-time imaging and precise alignment of the membrane under test.

To allow systematic optical characterization, the chip contains an array of sixteen 1×1 mm² suspended membranes with lithographically varied PtC radii, as illustrated in FIG. 4b. A reference region without a membrane (center tile) provides direct measurement of the bare DBR reflectivity. During measurement, the camera image (FIG. 4c) is used to position the IR probe spot on the suspended membrane while visually confirming membrane integrity and avoiding edges or defects.

Representative reflectivity spectra for two different PtC radii are shown in FIG. 4d. Each spectrum exhibits two prominent dips. The short-wavelength feature (1535–1545 nm) corresponds to the vertically confined cavity mode, and its position shifts noticeably when the hole radius is changed, reflecting the sensitivity of this mode to the membrane’s effective refractive index. In contrast, the longer-wavelength dip near 1555 nm originates from the DBR stack and remains spectrally fixed for all membrane designs, confirming that it is governed by the multilayer mirror rather than the patterned Si_3N_4 membrane.

The cavity mode, formed in the vertical air gap between the membrane and DBR, appears as the short-wavelength dip and shifts when the hole radius changes (500 nm vs. 510 nm). This shift reflects the change in the membrane’s effective refractive index as the air fill frac-

tion increases. In contrast, the DBR mode is dictated by the multilayer stack and remains spectrally invariant.

To identify the physical origin of these resonances, we performed finite-element simulations of the electric-field distribution (FIG. 4e–f). At the cavity resonance wavelength, the field is strongly localized within the air gap, forming a vertically confined Fabry–Pérot mode with a standing-wave pattern between the high-reflectivity DBR and the PtC membrane. This mode exhibits a narrow linewidth with measured FWHM of 2.55 nm, corresponding to an optical quality factor $Q_{\text{opt}} \approx 604$ and a finesse of ≈ 800 .

The longer-wavelength feature corresponds to a DBR mode that arises when light scattered by the patterned membrane acquires non-planar wavevectors. Although a bare DBR strongly reflects normally incident plane waves, the proximity of the PtC membrane introduces lateral scattering that generates off-axis and higher-order k -components. These components can penetrate the multilayer stack and form a band-edge-like optical mode primarily confined within the DBR, with only weak, evanescent coupling back into the membrane. Because this resonance is governed by in-plane scattering dynamics rather than the vertical cavity spacing, its spectral response remains fixed as the hole radius is varied. As a result, it appears as a broader, geometry-insensitive feature (FWHM 6.13 nm, $Q_{\text{opt}} \approx 254$) in the reflectivity spectrum.

Finally, FIG. 4d demonstrates spectral tunability across devices on the same chip: increasing the PtC hole radius results in a blue-shift of the cavity mode while leaving the DBR mode unchanged. This confirms that the membrane governs the cavity-mode position, while the DBR provides a stable, broadband bottom mirror unaffected by lithographic variations.

Overall, the combined experimental and simulated results confirm that the integrated platform functions as a stable, tunable, high-finesse cavity. The cavity mode’s strong out-of-plane localization makes it ideal for interferometric displacement sensing, while the coexistence of membrane and DBR modes offers opportunities for hybrid photonic-optomechanical architectures.

V. MECHANICAL RESONANCE CHARACTERIZATION AND HIGH-Q PERFORMANCE OF SUSPENDED MEMBRANE DEVICES

In the past several years, the isotropic SF_6 plasma undercut used here has emerged as one of the most powerful release techniques for Si_3N_4 , enabling devices with Q_{mech} approaching 10^9 – 10^{10} on standard silicon substrates. However, it has never been established whether integrating Si_3N_4 with a multilayer DBR—containing dozens of interfaces, different acoustic impedances, and altered boundary conditions—introduces mechanical loss or degrades dissipation dilution. Demonstrating Q preservation is therefore essential before this integration platform

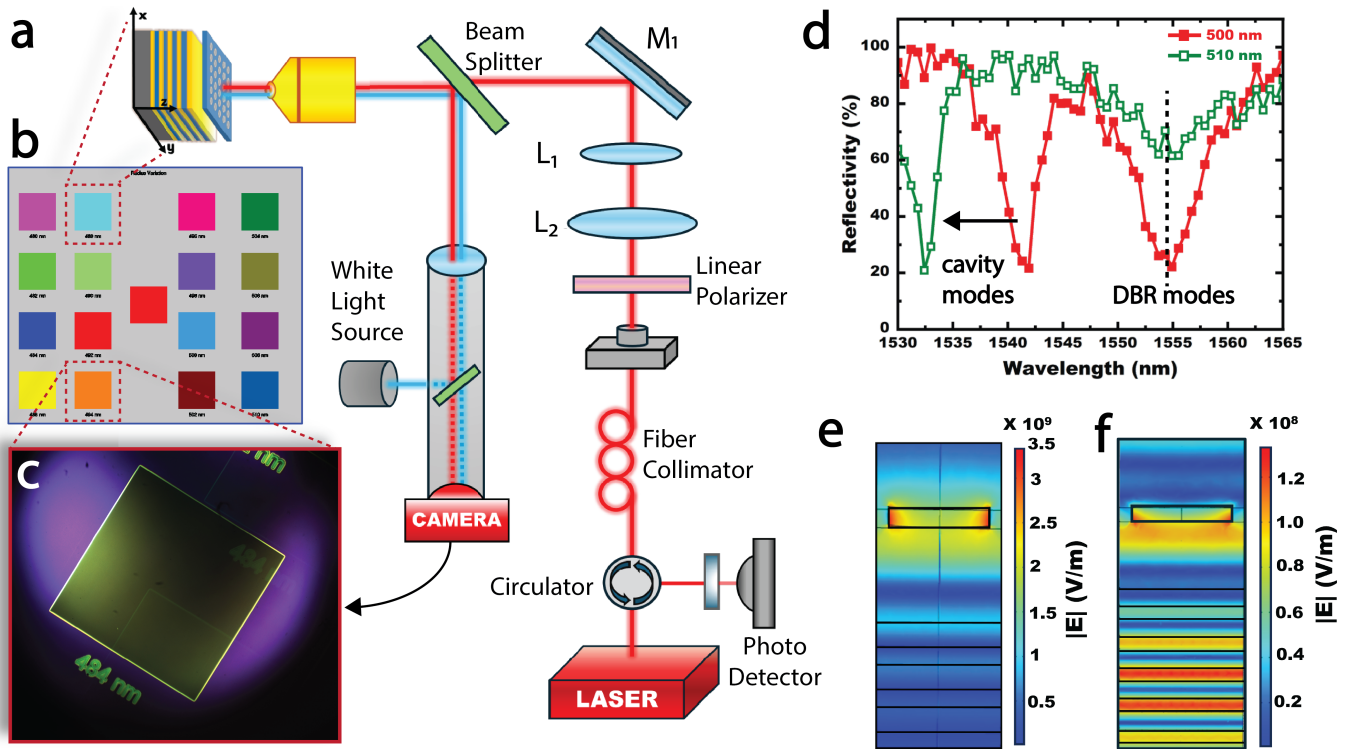


FIG. 4. Optical characterization of the integrated Si₃N₄-DBR cavity using broadband reflectivity measurements. (a) Schematic of the micro-reflectivity setup used for cavity measurements, combining a tunable IR laser for reflectivity spectroscopy with a white-light camera path for alignment. (b) Layout of the fabricated chip showing an array of sixteen 1×1 mm² suspended PtC membranes with lithographically varied hole radii, plus a central DBR-only reference region. (c) Camera image used during alignment, showing a suspended Si₃N₄ membrane under white-light illumination with the IR probe spot positioned at its center. (d) Measured reflectivity spectra for two membrane designs (500 nm and 510 nm hole radii). The cavity mode shifts with radius, while the DBR-associated mode remains fixed. (e) Simulated electric-field distribution of the vertically confined cavity mode formed in the air gap. (f) Simulated electric-field distribution of the DBR-associated photonic band-edge mode, confined mainly within the patterned membrane.

can be used for state-of-the-art optomechanically engineered geometries.

To evaluate this, we characterized DBR-integrated membranes using laser Doppler vibrometry (LDV) under high vacuum ($\approx 10^{-6}$ mbar). FIG. 5a shows the measured out-of-plane velocity field of the fundamental membrane mode, exhibiting the expected symmetric displacement profile. A broadband sweep (FIG. 5b) identifies the fundamental resonance near 259 kHz and several higher-order modes extending to 1 MHz. The fundamental peak was then isolated, and its decay was measured after abruptly switching off the piezo drive. The ring-down trace (FIG. 5c) yields a mechanical quality factor $Q_{\text{mech}} = 3.0 \times 10^5$, demonstrating low intrinsic damping and strong stress dilution.

Because the membranes used here are 200 nm thick (i.e. chosen to ensure high optical reflectivity), these Q_{mech} values are naturally lower than those achievable with ultra-thin (20 nm) Si₃N₄ films. Thicker mirrors are required for the PtC reflectivity, but multi-thickness designs can decouple these requirements (e.g., thick mirror region with thin, stress-diluted clamping) [4, 12]. Thus, it is important not only to measure the Q_{mech} of this sim-

ple square membrane, but to verify that DBR integration does not introduce additional loss. If Q_{mech} is preserved in this geometry, the platform can support the full family of high- Q_{mech} , phononic-engineered, soft-clamped, or tethered designs known to reach 10^8 - 10^{10} .

To assess the mechanical impact of DBR integration, we first identified the highest- Q_{mech} device on the DBR-integrated chip, corresponding to a hole radius of 484 nm. We then fabricated the nominally identical chip layout without DBR integration and directly compared the same membrane design (FIG. 4b). The DBR-integrated membrane exhibited a fundamental frequency of 259 kHz and $Q_{\text{mech}} = 3.0 \times 10^5$, while the corresponding membrane on silicon without DBR showed a slightly higher frequency of 290 kHz and $Q_{\text{mech}} = 3.8 \times 10^5$. The frequency shift is consistent with small variations in film thickness and thermal-expansion stresses associated with the DBR structure. Across the measured device sets, the average mechanical quality factors were $\langle Q_{\text{mech}} \rangle = 1.3 \times 10^5$ for the PhC+DBR devices and $\langle Q_{\text{mech}} \rangle = 4.6 \times 10^5$ for the PhC-only devices, indicating that the integrated structures remain within the same order of magnitude in mechanical coherence. Crucially,

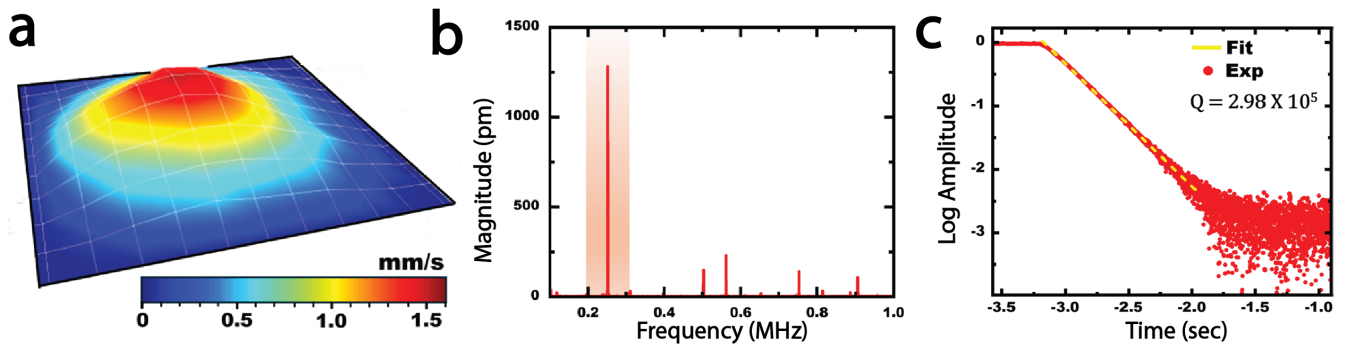


FIG. 5. Mechanical characterization of the suspended Si_3N_4 membrane integrated with a DBR platform. (a) Out-of-plane velocity map of the fundamental membrane mode measured by laser Doppler vibrometer. (b) Frequency-domain spectrum showing the fundamental resonance and higher-order modes. (c) Mechanical ringdown measurement of the fundamental mode, with an exponential fit (yellow) used to extract Q_{mech} .

no catastrophic degradation in Q_{mech} was observed upon DBR integration. Unlike soft-clamped modes, the fundamental modes of square membranes are strongly coupled to the substrate and therefore maximize chip-based loss channels, making them a stringent reference for assessing additional dissipation introduced by the DBR stack. [53]

These measurements demonstrate that the $\text{Si}_3\text{N}_4/\text{SiO}_2$ DBR introduces little additional mechanical loss. The SF_6 release process preserves the dissipation characteristics of the membrane even on a multilayer mirror substrate, confirming full compatibility with high-stress Si_3N_4 . This establishes the platform as a mechanically benign integration scheme capable of supporting the highest- Q geometries developed in the community while simultaneously enabling a compact, high-finesse optical cavity.

VI. CONCLUSION AND OUTLOOK

We have presented a scalable, CMOS-compatible fabrication strategy that monolithically integrates high-stress Si_3N_4 membranes with broadband distributed Bragg reflectors (DBRs) using a wafer-level, lithography-defined process. This platform removes a longstanding bottleneck in cavity optomechanics by eliminating bonding, through-wafer etching, and precision alignment. Instead, a stiction-free gas-phase undercut defines a vertically self-aligned cavity with uniform sub-micron membrane-DBR spacing. Vertical optomechanical coupling is especially well suited to Si_3N_4 , as its highest- Q_{mech} resonators exploit out-of-plane flexural modes defined by ultrathin film thicknesses (≈ 20 nm), which are straightforward to realize by deposition but extremely challenging to achieve through lateral nanolithography [51].

A central materials advance is the use of alternating LPCVD Si_3N_4 and SiO_2 layers to form a thermally robust DBR. Although the refractive-index contrast is lower than in $\text{Ta}_2\text{O}_5/\text{SiO}_2$ stacks, the LPCVD process yields exceptionally low optical absorption and remains

stable through the 800–900 °C required for stoichiometric high-stress Si_3N_4 deposition. In this way, lower index contrast is offset by low optical loss, enabling finesse values comparable to those demonstrated in higher-contrast III–V systems [48].

Optical and mechanical characterization confirms that integration preserves the essential performance of the Si_3N_4 platform. Mechanical ringdown measurements show $Q_{\text{mech}} > 10^5$, comparable to non-integrated membranes, while reflectivity spectra show cavity finesse above 800 and strong resonances suitable for precision optical readout. Although our demonstration uses relatively thick (200 nm) square membranes rather than geometries optimized for record Q_{mech} , the DBR process adds little mechanical loss compared to identical devices without DBR.

The fabrication route is broadly compatible with the wider ecosystem of Si_3N_4 resonators used in cavity optomechanics, including reflective phononic membranes [42], trampolines [12], hierarchical metamaterials, and high-aspect-ratio resonators [50]. It is also well suited to thick-substrate implementations, which are known to improve Q_{mech} for modes without soft clamping [12, 53, 54], since the SF_6 gas-phase release suspends membranes on millimeter-scale substrates in seconds while avoiding the stiction, bowing, and poor yield associated with wet-etch access through thick chips [32]. Previous strategies based on locally thickening the mirror region while thinning the clamping region to tens of nanometers [4, 12] should therefore be naturally extendable to this platform.

More broadly, the platform is compatible with the ultra-high-aspect-ratio geometries enabled by high-stress Si_3N_4 . Recent work has shown that centimeter-scale PtC reflectors with nanometer thickness and billions of holes can be fabricated with exceptional flatness [50]; at these scales, larger beam diameters can sustain high reflectivity even for thinner membranes [55]. Although we demonstrate a flat-flat cavity here, PtC structures with radially varying hole geometries can also impart effective curva-

ture [56, 57], offering future opportunities for transverse-mode engineering, reduced sensitivity to lateral misalignment, and lower clipping loss.

Taken together, this monolithic platform transforms a delicate, alignment-limited cavity optomechanical architecture into a robust and manufacturable one. By preserving the strong optical and mechanical performance of high-stress Si_3N_4 while replacing complex assembly with a simple self-aligned process, it provides a practical route toward scalable precision sensing, integrated photonics, and next-generation quantum technologies.

VII. METHODS

The DBR multilayer was fabricated by alternating low-pressure chemical vapor deposition (LPCVD) of SiO_2 and low-stress silicon nitride layers. The oxide films were deposited in a horizontal hot-wall LPCVD furnace at 700 °C and a pressure of 150 mTorr, using vaporized tetraethyl orthosilicate (TEOS) as the precursor. Low-stress silicon nitride layers were deposited in a similar furnace by introducing a mixture of NH_3 and dichlorosilane (DCS), with a fixed NH_3/DCS flow ratio of 0.19, corresponding to a Si-rich regime. The nitride deposition was carried out at 860 °C and 150 mTorr.

LPCVD was preferred over plasma-enhanced CVD (PECVD) for nitride deposition due to the negligible hydrogen incorporation associated with the former technique. The resulting low hydrogen content confers excellent thermal stability to the films, preventing significant stress variations as well as cracking or delamination during subsequent deposition steps.

After completion of the DBR stack, a 1 μm -thick amorphous silicon layer was deposited in an LPCVD reactor by flowing SiH_4 at 560 °C. The topmost high-stress silicon nitride layer was subsequently deposited in the same furnace used for the DBR nitride layers, but with a

substantially higher NH_3/DCS flow ratio corresponding to stoichiometric conditions. In this case, the deposition temperature and pressure were set to 700 °C and 150 mTorr, respectively.

ACKNOWLEDGMENTS

We thank Mohammadjavad Ebrahimipour, Juan Lizarraga Lallana for experimental help and Gerard Verbiest, Peter Steeneken, Andrea Cupertino and Dalziel Wilson for thoughtful comments. This work has received funding from the EMPIR programme co-financed by the Participating States and from the European Union’s Horizon 2020 research and innovation programme (No. 17FUN05 PhotoQuant). This publication is part of the project, Probing the physics of exotic superconductors with microchip Casimir experiments (740.018.020) of the research programme NWO Start-up which is partly financed by the Dutch Research Council (NWO). Funded/Co-funded by the European Union (ERC, EARS, 101042855). Views and opinions expressed are however those of the author(s) only and do not necessarily reflect those of the European Union or the European Research Council. Neither the European Union nor the granting authority can be held responsible for them.

CONFLICT OF INTEREST

The authors declare no conflict of interest.

DATA AVAILABILITY STATEMENT

The data that support the findings of this study are available from the corresponding author upon reasonable request.

-
- [1] M. Aspelmeyer, T. J. Kippenberg, and F. Marquardt, Cavity optomechanics, *Rev. Mod. Phys.* **86**, 1391 (2014).
- [2] B.-B. Li, L. Ou, Y. Lei, and Y.-C. Liu, Cavity optomechanical sensing, *Nanophotonics* **10**, 2799 (2021).
- [3] M. Rossi, D. Mason, J. Chen, Y. Tsaturyan, and A. Schliesser, Measurement-based quantum control of mechanical motion, *Nature* **563**, 53 (2018).
- [4] G. Huang, A. Beccari, N. J. Engelsen, and T. J. Kippenberg, Room-temperature quantum optomechanics using an ultralow noise cavity, *Nature* **626**, 512 (2024).
- [5] C. Reinhardt, T. Müller, A. Bourassa, and J. C. Sankey, Ultralow-noise sin trampoline resonators for sensing and optomechanics, *Phys. Rev. X* **6**, 021001 (2016).
- [6] B. P. Abbott, R. Abbott, T. D. Abbott, M. R. Abernathy, F. Acernese, K. Ackley, C. Adams, T. Adams, P. Addesso, R. X. Adhikari, *et al.*, Observation of gravitational waves from a binary black hole merger, *Physical Review Letters* **116**, 061102 (2016).
- [7] N. J. Engelsen, A. Beccari, and T. J. Kippenberg, Ultrahigh-quality-factor micro-and nanomechanical resonators using dissipation dilution, *Nature Nanotechnology* **19**, 725 (2024).
- [8] M. Xu, D. Shin, P. M. Sberna, R. van der Kolk, A. Cupertino, M. A. Bessa, and R. A. Norte, High-strength amorphous silicon carbide for nanomechanics, *Advanced Materials* **36**, 2306513 (2024).
- [9] A. T. Land, M. Dey Chowdhury, A. R. Agrawal, and D. J. Wilson, Sub-ppm nanomechanical absorption spectroscopy of silicon nitride, *Nano Letters* **24**, 7578 (2024).
- [10] J. Thompson, B. Zwickl, A. Jayich, F. Marquardt, S. Girvin, and J. Harris, Strong dispersive coupling of a high-finesse cavity to a micromechanical membrane, *Nat-*

- ture **452**, 72 (2008).
- [11] Y. Tsaturyan, A. Barg, E. S. Polzik, and A. Schliesser, Ultracoherent nanomechanical resonators via soft clamping and dissipation dilution, *Nature Nanotechnology* **12**, 776 (2017).
- [12] R. A. Norte, J. P. Moura, and S. Gröblacher, Mechanical resonators for quantum optomechanics experiments at room temperature, *Phys. Rev. Lett.* **116**, 147202 (2016).
- [13] A. H. Ghadimi, S. A. Fedorov, N. J. Engelsens, M. J. Beryhi, R. Schilling, D. J. Wilson, and T. J. Kippenberg, Elastic strain engineering for ultralow mechanical dissipation, *Science* **360**, 764 (2018).
- [14] D. Shin, A. Cupertino, M. H. de Jong, P. G. Steeneken, M. A. Bessa, and R. A. Norte, Spiderweb nanomechanical resonators via bayesian optimization: inspired by nature and guided by machine learning, *Advanced Materials* **34**, 2106248 (2022).
- [15] M. J. Beryhi, A. Arabmoheghi, A. Beccari, S. A. Fedorov, G. Huang, T. J. Kippenberg, and N. J. Engelsens, Perimeter modes of nanomechanical resonators exhibit quality factors exceeding 10^9 at room temperature, *Physical Review X* **12**, 021036 (2022).
- [16] D. J. Wilson, C. A. Regal, S. B. Papp, and H. J. Kimble, Cavity optomechanics with stoichiometric SiN films, *Phys. Rev. Lett.* **103**, 207204 (2009).
- [17] A. Cupertino, D. Shin, L. Guo, P. G. Steeneken, M. A. Bessa, and R. A. Norte, Centimeter-scale nanomechanical resonators with low dissipation, *Nature Communications* **15**, 4255 (2024).
- [18] A. G. Krause, M. Winger, T. D. Blasius, Q. Lin, and O. Painter, A high-resolution microchip optomechanical accelerometer, *Nature Photonics* **6**, 768 (2012).
- [19] M. H. De Jong, A. Ganesan, A. Cupertino, S. Gröblacher, and R. A. Norte, Mechanical overtone frequency combs, *Nature Communications* **14**, 1458 (2023).
- [20] D. Mason, J. Chen, M. Rossi, Y. Tsaturyan, and A. Schliesser, Continuous force and displacement measurement below the standard quantum limit, *Nature Physics* **15**, 745 (2019).
- [21] S. S. Verbridge, J. M. Parpia, R. B. Reichenbach, L. M. Bellan, and H. G. Craighead, High quality factor resonance at room temperature with nanostrings under high tensile stress, *Journal of Applied Physics* **99** (2006).
- [22] P. Sadeghi, M. Tanzer, S. L. Christensen, and S. Schmid, Influence of clamp-widening on the quality factor of nanomechanical silicon nitride resonators, *Journal of Applied Physics* **126** (2019).
- [23] S. Schmid, K. Jensen, K. Nielsen, and A. Boisen, Damping mechanisms in high-q micro and nanomechanical string resonators, *Physical Review B—Condensed Matter and Materials Physics* **84**, 165307 (2011).
- [24] D. Hoch, X. Yao, and M. Poot, Geometric tuning of stress in predisplaced silicon nitride resonators, *Nano Letters* **22**, 4013 (2022).
- [25] Z. Li, M. Xu, R. A. Norte, A. M. Aragón, P. G. Steeneken, and F. Aljani, Strain engineering of nonlinear nanoresonators from hardening to softening, *Communications Physics* **7**, 53 (2024).
- [26] M. J. Beryhi, A. Beccari, R. Groth, S. A. Fedorov, A. Arabmoheghi, T. J. Kippenberg, and N. J. Engelsens, Hierarchical tensile structures with ultralow mechanical dissipation, *Nature Communications* **13**, 3097 (2022).
- [27] E. Serra, B. Morana, A. Borrielli, F. Marin, G. Pandraud, A. Pontin, G. A. Prodi, P. M. Sarro, and M. Bonaldi, Silicon nitride mome oscillator for room temperature quantum optomechanics, *Journal of Microelectromechanical Systems* **27**, 1193 (2018).
- [28] L. G. Villanueva and S. Schmid, Evidence of surface loss as ubiquitous limiting damping mechanism in SiN micro- and nanomechanical resonators, *Phys. Rev. Lett.* **113**, 227201 (2014).
- [29] S. Chakram, Y. S. Patil, L. Chang, and M. Vengalattore, Dissipation in ultrahigh quality factor SiN membrane resonators, *Phys. Rev. Lett.* **112**, 127201 (2014).
- [30] P.-L. Yu, K. Cicak, N. Kampel, Y. Tsaturyan, T. Purdy, R. Simmonds, and C. Regal, A phononic bandgap shield for high-q membrane microresonators, *Applied Physics Letters* **104** (2014).
- [31] C. Reetz, R. Fischer, G. G. Assumpcao, D. P. McNally, P. S. Burns, J. C. Sankey, and C. A. Regal, Analysis of membrane phononic crystals with wide band gaps and low-mass defects, *Physical Review Applied* **12**, 044027 (2019).
- [32] R. A. Norte, *Nanofabrication for on-chip optical levitation, atom-trapping, and superconducting quantum circuits* (California Institute of Technology, 2015).
- [33] D. Høj, F. Wang, W. Gao, U. B. Hoff, O. Sigmund, and U. L. Andersen, Ultra-coherent nanomechanical resonators based on inverse design, *Nature communications* **12**, 5766 (2021).
- [34] M. Yuan, M. A. Cohen, and G. A. Steele, Silicon nitride membrane resonators at millikelvin temperatures with quality factors exceeding 108, *Applied Physics Letters* **107** (2015).
- [35] T. Purdy, R. Peterson, P. Yu, and C. Regal, Cavity optomechanics with Si_3N_4 membranes at cryogenic temperatures, *New Journal of Physics* **14**, 115021 (2012).
- [36] W.-H. Chuang, T. Luger, R. K. Fetting, and R. Ghodssi, Mechanical property characterization of SiN thin films at cryogenic temperatures, *Journal of Microelectromechanical Systems* **13**, 870 (2004).
- [37] Y. Seis, T. Capelle, E. Langman, S. Saarinen, E. Planz, and A. Schliesser, Ground state cooling of an ultracoherent electromechanical system, *Nature Communications* **13**, 1507 (2022).
- [38] R. Fischer, N. Kampel, G. Assumpção, P.-L. Yu, K. Cicak, R. Peterson, R. Simmonds, and C. Regal, Optical probing of mechanical loss of a SiN membrane below 100 mK, arXiv preprint arXiv:1611.00878 (2016).
- [39] F. Zhou, Y. Bao, J. J. Gorman, and J. R. Lawall, Cavity optomechanical bistability with an ultrahigh reflectivity photonic crystal membrane, *Laser & photonics reviews* **17**, 2300008 (2023).
- [40] F. Zhou, Y. Bao, J. Gorman, and J. R. Lawall, Ultrahigh reflectivity photonic crystal membranes with optimal geometry, *APL Photonics* **9** (2024).
- [41] M. H. de Jong, J. Li, C. Gärtner, R. A. Norte, and S. Gröblacher, Coherent mechanical noise cancellation and cooperativity competition in optomechanical arrays, *Optica* **9**, 170 (2022).
- [42] G. Enzian, Z. Wang, A. Simonsen, J. Mathiassen, T. Vibel, Y. Tsaturyan, A. Tagantsev, A. Schliesser, and E. S. Polzik, Phononically shielded photonic-crystal mirror membranes for cavity quantum optomechanics, *Optics Express* **31**, 13040 (2023).
- [43] X. Chen, C. Chardin, K. Makles, C. Caër, S. Chua, R. Braive, I. Robert-Philip, T. Briant, P.-F. Cohadon, A. Heidmann, *et al.*, High-finesse fabry-perot cavities

- with bidimensional si_3n_4 photonic-crystal slabs, *Light: Science & Applications* **6**, e16190 (2017).
- [44] V. Dumont, S. Bernard, C. Reinhardt, A. Kato, M. Ruf, and J. C. Sankey, Flexure-tuned membrane-at-the-edge optomechanical system, *Optics express* **27**, 25731 (2019).
- [45] C. H. Bui, J. Zheng, S. Hoch, L. Y. Lee, J. Harris, and C. Wei Wong, High-reflectivity, high-q micromechanical membranes via guided resonances for enhanced optomechanical coupling, *Applied Physics Letters* **100** (2012).
- [46] T. Mitra, G. Singh, A. A. Darki, S. P. Madsen, and A. Dantan, Narrow-linewidth fano microcavities with resonant subwavelength grating mirror, *Optics Express* **32**, 15667 (2024).
- [47] A. D. Hyatt, O. A. Flores, A. R. Agrawal, C. A. Condos, and D. J. Wilson, Fabrication and characterization of high-q silicon nitride membrane resonators, *Journal of Visualized Experiments (JoVE)*, e68706 (2025).
- [48] S. Kini Manjeshwar, A. Ciers, J. Monsel, H. Pfeifer, C. Peralle, S. M. Wang, P. Tassin, and W. Wieczorek, Integrated microcavity optomechanics with a suspended photonic crystal mirror above a distributed bragg reflector, *Optics Express* **31**, 30212 (2023).
- [49] G. J. Hornig, S. Al-Sumaidae, J. Maldaner, L. Bu, and R. DeCorby, Monolithically integrated membrane-in-the-middle cavity optomechanical systems, *Optics Express* **28**, 28113 (2020).
- [50] L. Norder, S. Yin, M. H. de Jong, F. Stallone, H. Aydogmus, P. M. Sberna, M. A. Bessa, and R. A. Norte, Pentagonal photonic crystal mirrors: scalable lightsails with enhanced acceleration via neural topology optimization, *Nature Communications* **16**, 2753 (2025).
- [51] J. Guo, R. Norte, and S. Gröblacher, Feedback cooling of a room temperature mechanical oscillator close to its motional ground state, *Physical review letters* **123**, 223602 (2019).
- [52] M. Xu, R. J. Elbertse, A. Keşkekler, G. Bimonte, J. Lee, S. Otte, and R. A. Norte, Measuring casimir force across a superconducting transition, *arXiv preprint arXiv:2504.10579* (2025).
- [53] M. H. de Jong, M. A. ten Wolde, A. Cupertino, S. Gröblacher, P. G. Steeneken, and R. A. Norte, Mechanical dissipation by substrate-mode coupling in sin resonators, *Applied Physics Letters* **121** (2022).
- [54] D. J. Wilson, *Cavity optomechanics with high-stress silicon nitride films* (California Institute of Technology, 2012).
- [55] J. P. Moura, R. A. Norte, J. Guo, C. Schäfermeier, and S. Gröblacher, Centimeter-scale suspended photonic crystal mirrors, *Optics express* **26**, 1895 (2018).
- [56] A. Agrawal, J. Manley, D. Allepuz-Requena, and D. Wilson, Focusing membrane metamirrors for integrated cavity optomechanics, *Optica* **11**, 1235 (2024).
- [57] J. Guo, R. A. Norte, and S. Gröblacher, Integrated optical force sensors using focusing photonic crystal arrays, *Optics express* **25**, 9196 (2017).